Role for a Cindr–Arf6 axis in patterning emerging epithelia

Ruth I. Johnson[a,*], Alanna Sedgwick[b], Crislyn D'Souza-Schorey[b], and Ross L. Cagan[a]
[a]Department of Developmental and Regenerative Biology, Mount Sinai School of Medicine, New York, NY 10029;
[b]Department of Biological Sciences, University of Notre Dame, Notre Dame, IN 46556

ABSTRACT **Patterning of the *Drosophila* pupal eye is characterized by precise cell movements. In this paper, we demonstrate that these movements require an Arf regulatory cycle that connects surface receptors to actin-based movement. dArf6 activity—regulated by the Arf GTPase–activating proteins (ArfGAPs) dAsap and dArfGAP3 and the Arf GTP exchange factors Schizo and dPsd—promoted large cellular extensions; time-lapse microscopy indicated that these extensions presage cell rearrangements into correct epithelial niches. During this process, the *Drosophila* eye also requires interactions between surface Neph1/nephrin adhesion receptors Roughest and Hibris, which bind the adaptor protein Cindr (CD2AP). We provide evidence that Cindr forms a physical complex with dArfGAP3 and dAsap. Our data suggest this interaction sequesters ArfGAP function to liberate active dArf6 elsewhere in the cell. We propose that a Neph1/nephrin–Cindr/ArfGAP complex accumulates to limit local Arf6 activity and stabilize adherens junctions. Our model therefore links surface adhesion via an Arf6 regulatory cascade to dynamic modeling of the cytoskeleton, accounting for precise cell movements that organize the functional retinal field. Further, we demonstrate a similar relationship between the mammalian Cindr orthologue CD2AP and Arf6 activity in cell motility assays. We propose that this Cindr/CD2AP-mediated regulation of Arf6 is a widely used mechanism in emerging epithelia.**

Monitoring Editor
Alpha Yap
University of Queensland

Received: Apr 8, 2011
Revised: Sep 27, 2011
Accepted: Sep 29, 2011

INTRODUCTION

As organs emerge, they require the precise placement of their constituent cells to assemble functional structures. This process requires the integration of multiple processes, including changes in adhesion and cell shape, as well as precise long-range or local cell movements. Elements of these dynamic and strictly regulated processes have been studied in model systems both in vitro and in vivo (reviewed in Vicente-Manzanares *et al*. [2005]; Le Clainche and Carlier [2008]). Several factors have been identified that are required for migration of individual cells (e.g., vertebrate neural crest cells) or groups of cells (e.g., *Drosophila* border cells) that travel over or through surrounding tissues to specific destinations (reviewed in Aman and Piotrowski [2009]; Rorth [2009]). However, few studies have addressed the fundamental problem of how specific cell types integrated within a complex tissue layer are capable of reorganizing to generate a functional organ, a basic aspect of epithelial maturation.

The *Drosophila* pupal eye is an ideal model for exploring these issues in vivo. It is a postmitotic, pseudostratified neuroepithelium with multiple cell types that can be recognized based on their position (Cagan, 2009). Emerging "ommatidia" are spaced across the eye epithelium and, in the young pupa, are separated by a pool of initially undifferentiated interommatidial precursor cells (IPCs) that rearrange into a honeycomb lattice; their ordered local cell movements form the basis of our studies. Intercalation and later maturation of IPCs is in part mediated by the Ig-CAM proteins Roughest (Rst, the Neph1 orthologue) and Hibris (Hbs, orthologous to nephrin) that reside at adherens junctions (AJs; reviewed in Tepass and Harris [2007]). Expressed in different cell populations, Rst and Hbs bind preferentially to each other in a *trans* interaction (Bao and Cagan, 2005). We have previously

This article was published online ahead of print in MBoC in Press (http://www.molbiolcell.org/cgi/doi/10.1091/mbc.E11-04-0305) on October 5, 2011.

*Present address: Biology Department, Wesleyan University, Middletown, CT 06459.
Address correspondence to: Ross L. Cagan (ross.cagan@mssm.edu).

Abbreviations used: 1°s, primary pigment cell; 2°s, secondary pigment cells; 3°s, tertiary pigment cells; AJ, adherens junction; ArfGAP, Arf GTPase activating protein; ArfGEF, Arf GTP exchange factor; Cindr, CD2AP and CIN85 orthologue; EGFR, epidermal growth factor receptor; ER, endoplasmic reticulum; GFP, green fluorescent protein; GST, glutathione *S*-transferase; h APF, hours after puparium formation; Hbs, Hibris; IPCs, interommatidial precursor cells; MDCK, Madin-Darby canine kidney; OMS, ommatidial mispatterning score; RNAi, RNA interference; Rst, Roughest; SH3, Src homology 3.

demonstrated that the *Drosophila* CD2AP orthologue Cindr functions with Rst and Hbs to correctly pattern the developing eye: Cindr is required to regulate cytoskeletal changes that in turn coordinate cell movement; decreasing *cindr* increased motility and impeded cells from stably occupying their appropriate niches (Johnson *et al.*, 2008). In this paper, we demonstrate a direct, functional link between Cindr and two Arf GTPase-activating proteins (ArfGAPs) that target Arf6 for inactivation.

Of the multiple Arfs encoded in the mammalian and *Drosophila* genomes (reviewed in Gillingham and Munro [2007]), Arf6 alone has consistently been shown to localize to the plasma membrane and to regulate the actin cytoskeleton to promote PIP2-rich membrane protrusions and Rac1-dependent membrane ruffling and migration (Donaldson, 2003; Sabe, 2003; Claing, 2004; D'Souza-Schorey and Chavrier, 2006). Arf6 is known to be activated by multiple Arf GTP exchange factor (ArfGEFs), including GEP100, as well as several ArfGAPs, including ASAP, GIT1, and Centaurin ß1 (Gillingham and Munro, 2007); our data presented here indicate that *Drosophila* ArfGAP3 also regulates dArf6.

Though its role in cell movement in vivo is poorly understood, the regulation of Arf6 has become the subject of increased interest with the recent demonstration that it can promote metastasis in animal melanoma and glioma models; furthermore, Arf6 expression levels correlate with invasiveness of several breast tumor cell lines, and GEP100 has been similarly linked to breast cancer metastasis (Morishige *et al.*, 2008). In this work, we explore the role of dynamically regulated Arf pathway activity in directing the epithelial cell movements that pattern the pupal eye epithelium. We identify the *Drosophila* ArfGAP proteins dArfGAP3 and dAsap as novel Cindr interactors and demonstrate that they act as part of a cascade initiated at the cell surface that promotes directed cell movement of IPCs.

RESULTS

dArf6 activity is required for cell intercalation during *Drosophila* eye patterning

Commencing 18 h after puparium formation (h APF), two cells are selected as primary pigment cells (1°s) to enwrap each ommatidial cluster (Supplemental Movie S1). Between each ommatidial group is an excess of undifferentiated IPCs. As 1°s begin to enwrap the ommatidia—surrounding four, central, characteristically arranged cone cells and the underlying photoreceptor cells—IPCs progressively rearrange to generate a precise honeycomb lattice that will eventually organize the ommatidial array across the eye field; the IPCs themselves differentiate into secondary (2°) or tertiary (3°) pigment cells as excess cells are removed by apoptosis (Figure 1, A and C, and Movie S1). Movement by an IPC is initiated at the apical surface by extension of a thin process toward its target; stable apical contacts are then extended basally as the cell fully establishes its new position (Figure 1B; Cagan and Ready, 1989). By 40–42 h APF all cells have acquired final characteristic shapes and sizes, and the pattern is mature (Ready *et al.*, 1976; Miller and Cagan, 1998).

The actin cytoskeleton is extensively remodeled during the process of eye patterning (Johnson *et al.*, 2008). Previous studies have linked Arf6 to dynamic actin remodeling for the movement of cells in culture (Donaldson, 2003; D'Souza-Schorey and Chavrier, 2006). Using RNA interference (RNAi), we imaged *GMR>dArf6^{RNAi}* retinas in situ during the critical period of cell rearrangement (20–24 h APF; Movies S2–S4 and Figure 1D). In developing wild-type eyes (Movie S1 and Figure 1C), time-lapse microscopy revealed that IPCs intercalated into single rows by pushing between adjacent cells to extend to nonneighboring 1°s. Once these large projections reached a target 1°, they seldom retracted. Subsequent to this, the IPC:1° interface rapidly widened, and the cell body promptly shifted to stably occupy the niche.

dArf6^{RNAi} IPCs exhibited anemic cell extensions that seldom extended sufficiently far to reach a target 1° and were often retracted. When contact was occasionally achieved, the IPC:1° interface failed to rapidly widen and was commonly lost. Rather than generating one concerted extension, *dArf6^{RNAi}* IPCs typically produced multiple small extensions (Movie S2 and Figure 1D) or none at all (Movies S3 and S4). Reducing *dArf6* also induced some ectopic apoptosis prior to 20 h APF (Supplemental Figure S1, A and B), so we limited our live-imaging efforts at exploring cell intercalation to regions where multiple rows of cells lay between ommatidia. Impaired cell intercalation disrupted the final arrangement of cells in mature *dArf6^{RNAi}* eyes: few 2° and 3° niches were correctly occupied, IPCs frequently clustered into multiple rows, and the IPC lattice was poorly organized, leading to "fusion" of some ommatidia (Figure 2, A–E). Minor defects in cone and 1° cell organization and orientation were also present at low frequency (Figure 2).

We validated a role for Arf6 in patterning through several approaches. The same patterning defects were observed when independent RNAi-based transgenes that target three different regions of the *dArf6* transcript were expressed. The severity of these phenotypes, quantified as an "ommatidial mispatterning score" (OMS; see *Materials and Methods*; Johnson and Cagan, 2009) emphasized that the number of defects (4.1–5.2 errors per ommatidium) closely correlated with the degree of transcript knockdown (Figure 2, B–G, and Supplemental Tables S1 and S2). Additionally, *dArf6^{RNAi}* mispatterning was enhanced in retinas heterozygous for the mutant allele *dArf6^{KO1}* (Figure 2H), similar phenotypes were observed when dominant negative *dArf6* was expressed (Figure 2I), and *dArf6^{RNAi}* mispatterning and apoptosis were partially suppressed by ectopic dArf6 (Figure S1, C–E).

Drosophila Ig-CAM family proteins were functionally linked to *Arf6* patterning

Rst/Hbs interactions mediate final niche acquisition, cell shape, and pattern stabilization of IPCs (Bao and Cagan, 2005); genotypically *rst*$^{-}$ IPCs failed to move robustly and intercalate into new positions within the epithelium (Reiter *et al.*, 1996; Larson *et al.*, 2008). Early in the IPC patterning process, Hbs and Rst accumulate at the interface between 1°s and IPCs, respectively, as Rst fades from the labile IPC:IPC boundaries (Reiter *et al.*, 1996; Bao and Cagan, 2005). To address whether Rst/Hbs is functionally linked to dArf6 activity, we reduced *rst* or *hbs* genomic copy number in a *dArf6^{RNAi}* background. Patterning defects were enhanced (Figure 3, A–D), indicating a functional interaction among Arf6, Rst, and Hbs during IPC patterning. Quantitating these defects indicated a modest but statistically significant enhancement of *dArf6^{RNAi}* mispatterning in *rst* or *hbs* heterozygotes (Figure 3E and Table S3).

Multiple ArfGAPs and ArfGEFs are required for patterning

The fact that dArf6 is required for regulation of cell movements led us to explore the mechanisms that regulate this dynamic process. Candidate regulators include the *Drosophila* ArfGAP orthologues of mammalian ASAP (we refer to as *dAsap*, *CG30372*) and ArfGAP3 (*dArfGAP3*, *CG6838*; Figure S2A); we similarly explored the ArfGEF orthologues PSD (*dPsd/dEfa6*, *CG31158*) and GEP100 (*Schizo*, *siz*; Chen *et al.*, 2003; Onel *et al.*, 2004). *dArf6* and each of these proteins were ubiquitously expressed in the eye. Endogenous green

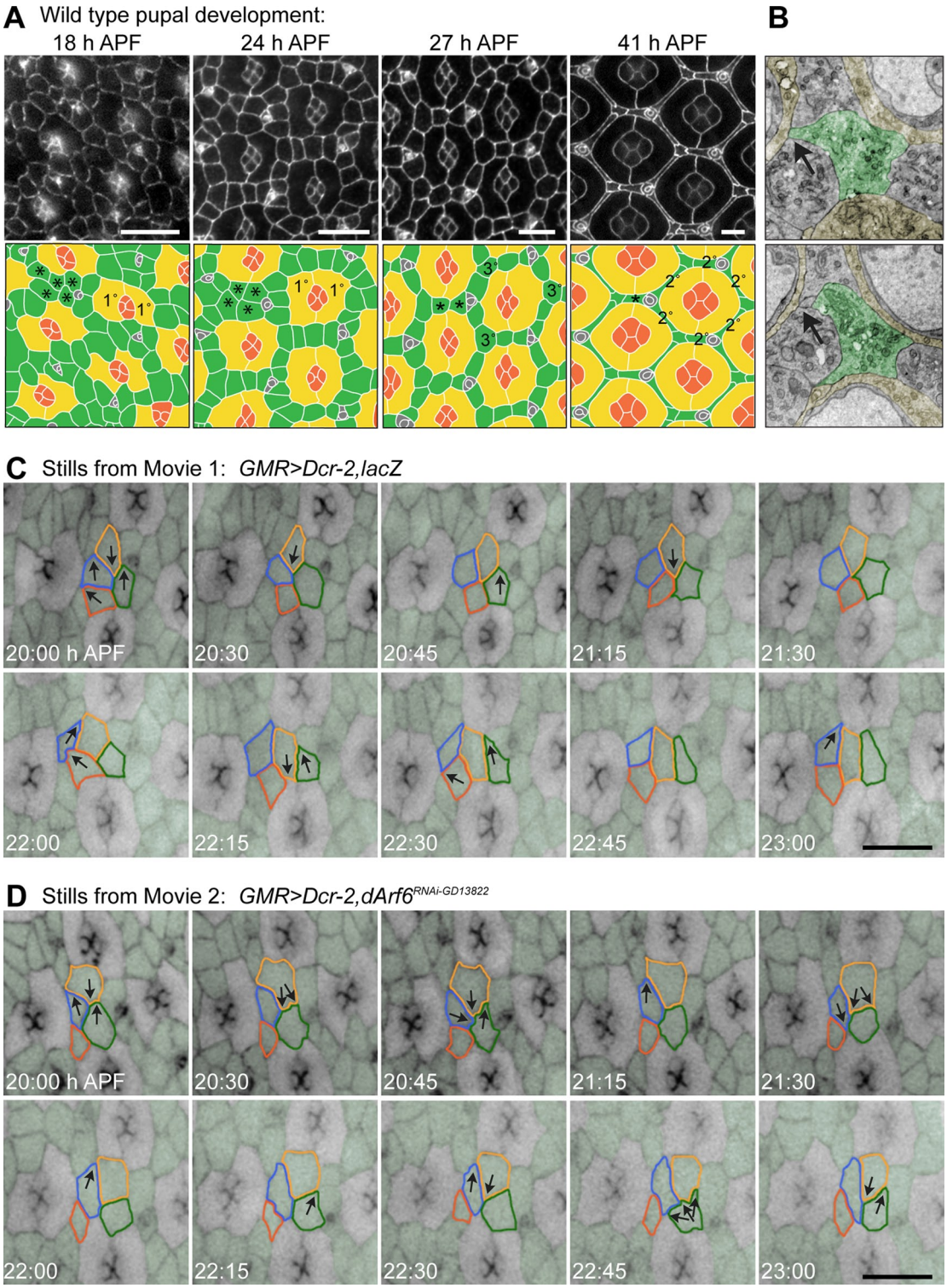

FIGURE 1: Patterning of the *Drosophila* eye requires dArf6. (A) Wild-type pupal eyes dissected at 18, 24, 27, and 41 h APF. α-DE-Cadherin labels AJs (top panels); bottom panels are tracings with cone cells in orange, 1°s in yellow, and IPCs in green. IPCs intercalate into single rows (compare cells labeled *), and excess cells are eliminated by apoptosis, leaving six 2°s arranged in a hexagon around each ommatidium (labeled in 41 h APF), with three 3°s at the vertices (labeled in 27h APF), alternating with bristle groups (in gray). (B) Electron micrographs of a single region between ommatidia. At the surface (top) a single IPC (green) has extended (arrow) to contact a third 1° (brown). At 2 μM more basally (bottom panel), this contact has yet to be extended. (C) Selected frames from Movie S1, which recorded wild-type intercalation of IPCs (genotype: *GMR, Dcr-2 >lacZ*). Developmental time points of each still are indicated. IPCs are pseudocolored green. Cells outlined in color pushed toward opposite ommatidia (arrows) to establish stable contacts that widened rapidly. (D) In age-matched *GMR, Dcr-2 >dArf6^{RNAi}* eye intercalation was slow and disordered. Cells repeatedly extended processes in multiple directions (arrows) and contacts with 1° cells were not secured laterally. Scale bars: 10 μm.

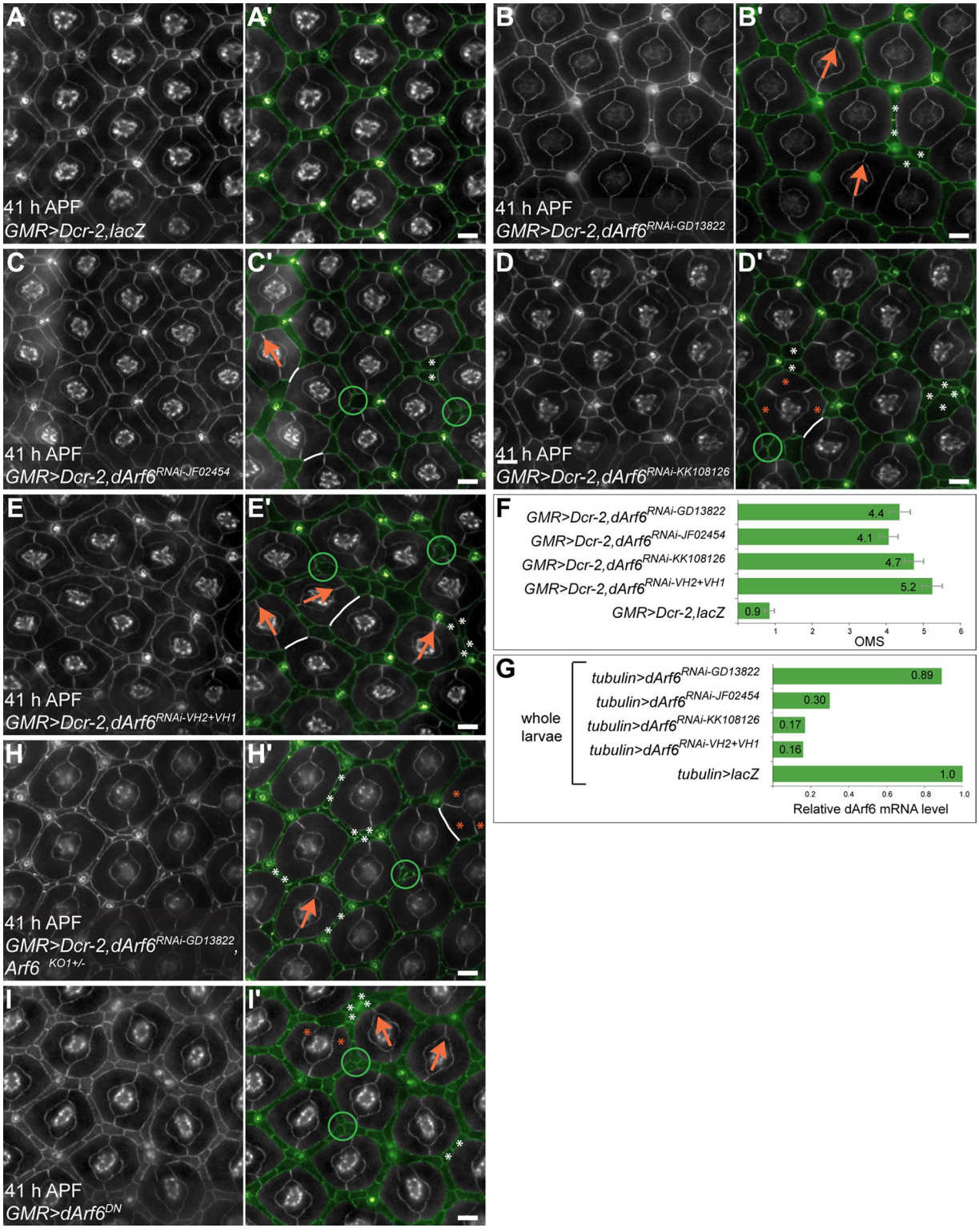

FIGURE 2: Reducing *dArf6* disrupts eye patterning. The mature pattern (A) was perturbed when dArf6 activity was reduced by expression of different independent $dArf6^{RNAi}$ transgenes. (B′–E′) In the right-hand panels, all IPCs are pseudocolored green and examples of characteristic defects are highlighted: errors in 1° cell number or morphology (orange *), misalignment of ommatidia (orange arrows), unresolved 3° niches (green circles), multiple cells within a 2° niche (white *), and immediately adjoining ommatidia (white lines). The hexagonal arrangement of the IPC lattice is distorted. (F) Quantification of the mean number of patterning errors observed per ommatidial hexagon (OMS) for genotypes shown in (D and E). Error bars represent SE; refer to Table S1 for detailed analyses. (G) Graph of relative transcript reduction (determined by qPCR) when these RNAi transgenes were driven in the whole larvae (see also Table S2). (H) Mispatterning generated by $dArf6^{RNAi}$ was enhanced in a *dArf6* null heterozygote; compare with (B). (I) Expression of $dArf6^{DN}$ phenocopied $dArf6^{RNAi}$. All eyes were dissected at 41 h APF. α-DE-cadherin labels AJs. All IPCs are pseudocolored green. Scale bars: 10 μm.

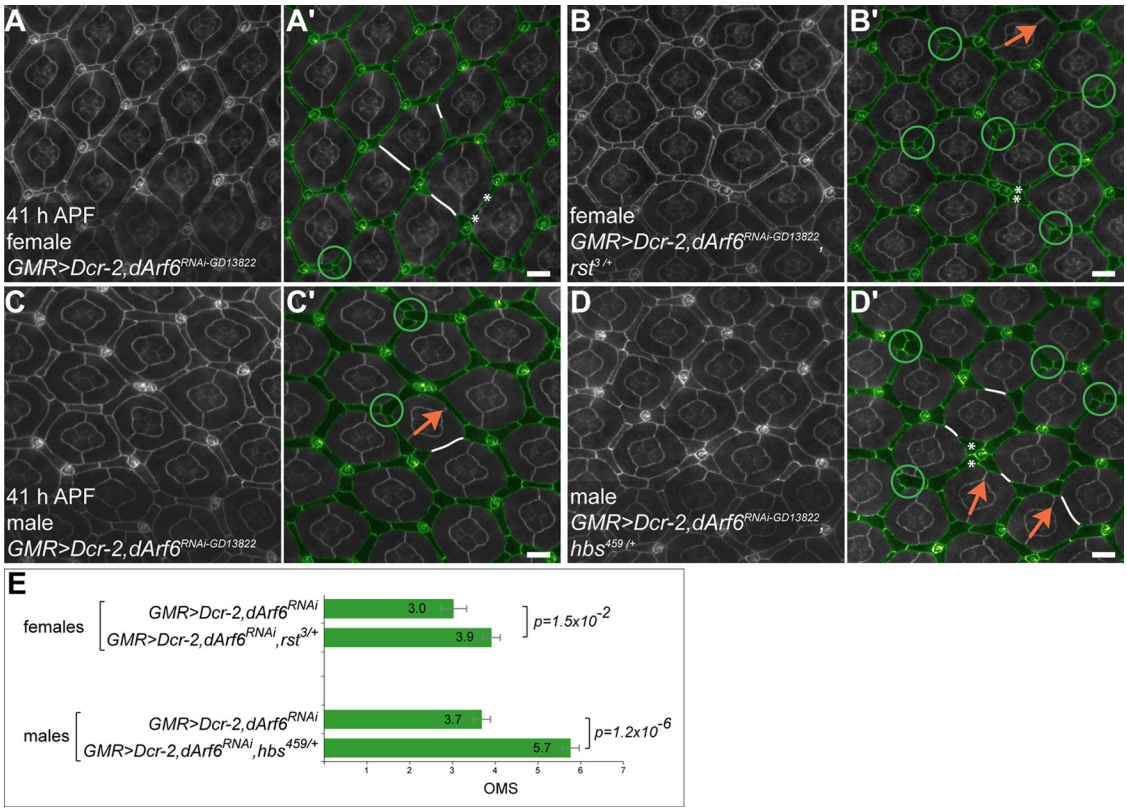

FIGURE 3: *dArf6* interacts with *Rst* and *Hbs*. *dArf6*$^{RNAi\text{-}GD13822}$ patterning defects (A) and (C) were mildly enhanced by removing an allele of the Ig-CAMs Rst (B) or Hbs (D). The interaction with *rst* (located on the X chromosome) was examined in female pupae; all other panels in this manuscript show tissue dissected from male pupae. In A′–D′, IPCs are pseudocolored green and several characteristic patterning errors are highlighted as described in Figure 2. All tissue was dissected at 41 h APF; α-DE-cadherin labels AJs. (E) Graph of the mean number of patterning errors (OMS) observed in these statistically significant genetic interactions (p values indicated). Error bars represent SE. Refer to Table S3 for detailed analyses. Scale bars: 10 μm.

fluorescent protein (GFP)-tagged dArf6 was uniformly distributed in IPCs during intercalation (Figures 4, A and B, and S3, A–C). In contrast, endogenous and ectopic dAsap and dArfGAP3 localized to numerous cytoplasmic and membrane-associated puncta (Figures 4C, S2, B and C, and S3, D–F). dPsd^{GFP} puncta were primarily associated with IPC junctions (Figures 4D and S3, G–I). As eye patterning progressed, Arf6, dAsap, and dArfGAP3 increased and accumulated at IPC AJs (Figure S3, J–L; unpublished data.

By targeting RNAi constructs to the developing eye, we determined that each of these loci was required for directed cell movement during IPC patterning (Figure 4, E–I): 2° and 3° niches were poorly resolved, the interweaving lattice frequently distorted into a pentagon or even a square between ommatidia, and occasional defects in cone cell arrangement and ommatidial orientation were also observed. These phenotypes phenocopied those observed when *dArf6* was reduced (Figure 2). Similar phenotypes were observed with multiple independent transgenes that targeted *dArfGAP3* and *dAsap*, and the severity of patterning errors correlated with the relative level of transcript reduction (Tables S1 and S2 and Figure S4). For example, reducing *dArfGAP3* transcripts to 38% of wild-type levels resulted in 3.4 errors per hexagon; further reduction (to 21%) led to 4.1 errors per hexagon. Reducing *dAsap* mRNA to 33% caused 2.8 errors per hexagon, while reduction to 16% resulted in 6.7 patterning errors per hexagon. Strong reduction of *dPsd* caused degenerative phenotypes—further studies are required to explore possible roles for dPsd in signal transduction and cell survival (Figure S4H). Mild reduction of *dPsd* and *siz* caused similar defects in patterning (Figure S4, I and J). Flies homozygous for a hypomorphic *dArfGAP3* allele that survived to 27 h APF also displayed mild eye-patterning defects (Figure 4, J and K). No alleles were available to generate viable, hypomorphic *dAsap*, *siz*, or *dPsd* eye tissue. These data indicate that the Arf-class regulators dArfGAP3, dAsap, Siz, and dPsd are each required for correct patterning of the eye and accomplish this in part through their regulation of IPC positioning.

Genetic evidence that dArfGAP3, dAsap, Siz, and dPsd regulate dArf6

dArf6^{RNAi} eye mispatterning was significantly enhanced in *dArfGAP3*, *dAsap*, *siz*, or *dPsd* heterozygotes (Figure 5, A–F), indicating a functional interaction between these loci in IPCs. Detailed analyses of specific patterning defects indicated that in each case the number of correctly patterned 2° and 3° cells was reduced (Table S3). The total number of IPCs did not differ markedly from the wild-type number of 12, indicating that the enhancement was due specifically to increased disorder in IPC patterning. Additionally, errors in the placement of three bristle groups about each ommatidium and errors in 1° and cone cell patterning and ommatidial rotation were modestly enhanced (compare with Figure 1A). These data are consistent with the view that dArf6 is regulated by dArfGAP3, dAsap, Siz, and dPsd to promote the normal cell intercalations and movements required for correct IPC patterning.

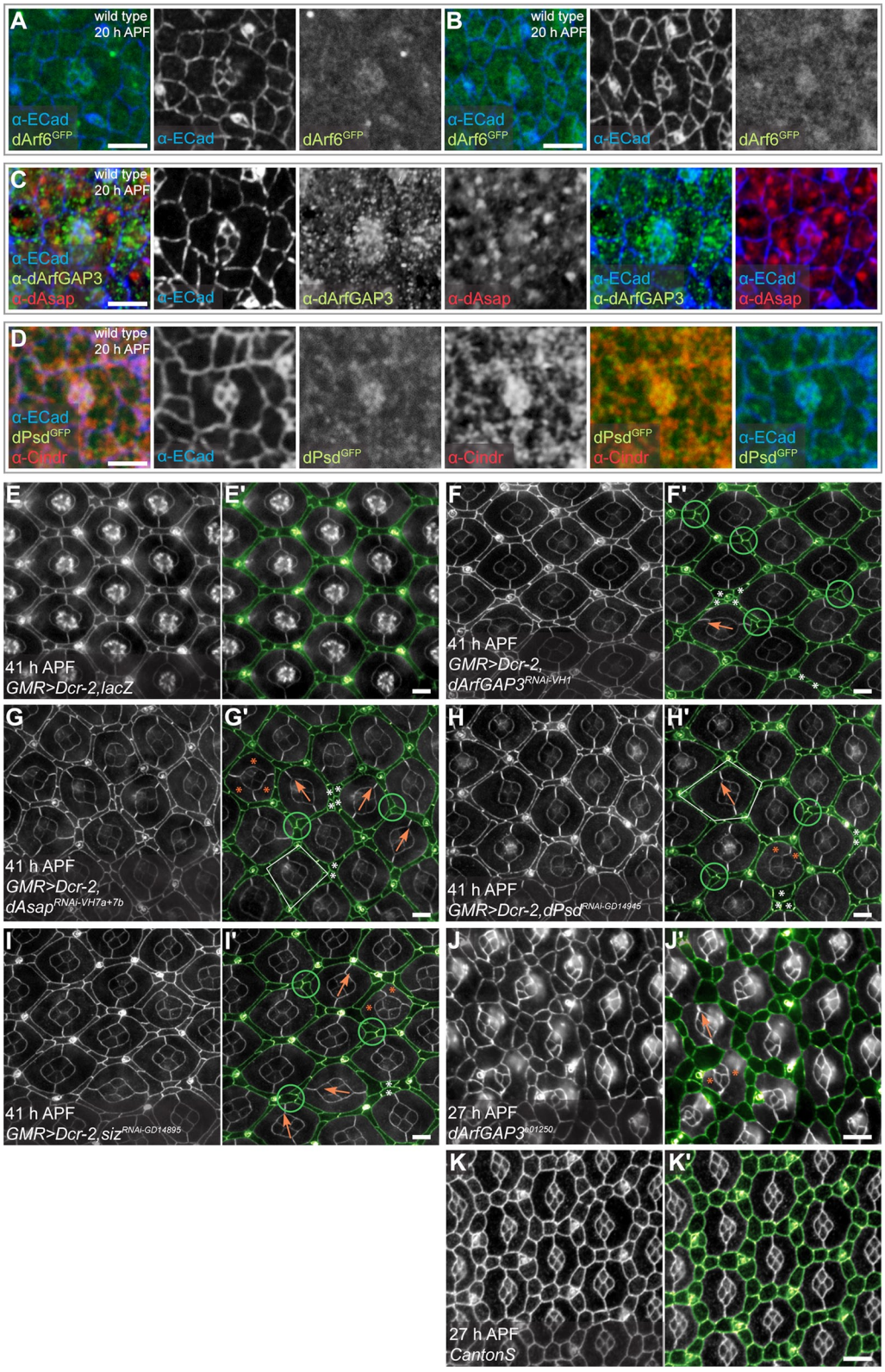

FIGURE 4: An Arf-regulation cycle is required for correct eye patterning. (A and B) Two examples of endogenous dArf6^{GFP} (green and far right panels). (C) Apical ArfGAP3 (green) partially colocalized with dAsap (red) and was also detected in large puncta basal to AJs. (D) Endogenous dPsd^{GFP} (green) localized to numerous puncta at the AJ and partially colocalized with Cindr (red). Eyes in (A–D) were dissected at 20 h APF; α-DE-cadherin marks AJs (blue and left panels). Wild-type patterning (E) was perturbed by RNAi transgenes targeting (F) *dArfGAP*, (G) *dAsap*, (H) *dPsp*, or (I) *siz*, and in (J) *dArfGAP3*^{e01250} homozygotes that survived to 27h APF—compare with patterning in age-matched tissue (K). Eyes were dissected at times indicated. α-DE-cadherin labels AJs. Characteristic patterning errors are highlighted as described in Figure 2; in additional, select ommatidia in G′, H′ have been outlined in white to emphasize distortion of the hexagonal shape. (A–D) Scale bars: 5 μm. (E–K) Scale bars: 10 μm.

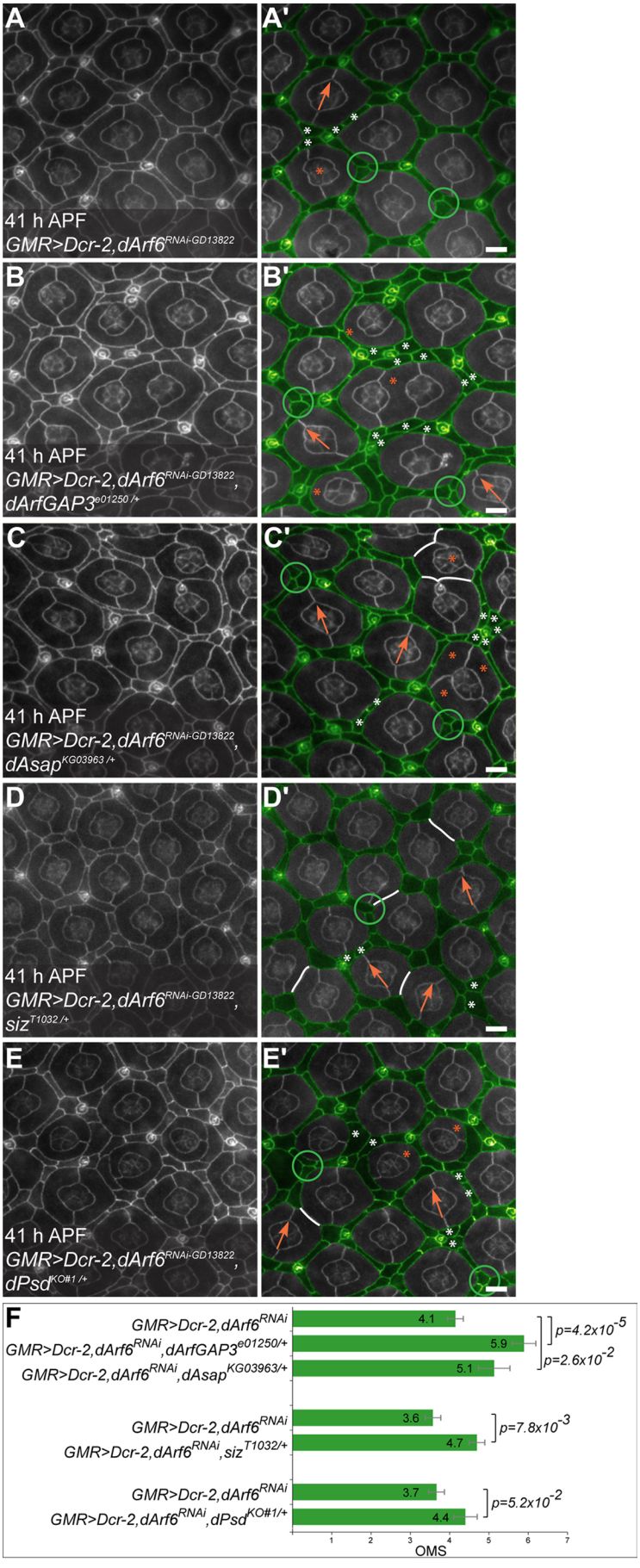

dArf6 is likely to regulate cell movement by influencing actin dynamics

Mammalian Arf6 can regulate actin cytoskeleton dynamics through several pathways: activation of PLD or PIP5-kinase, recruitment of RacGEFs to the plasma membrane, binding to the Rac effector Arfaptin, etc. (reviewed in Donaldson and Honda [2005]; Jaworski [2007]; Randazzo *et al*. [2007]; Ha *et al*. [2008]). In *Drosophila* embryos, dArf6 promotes localization and activation of Rac, which regulates actin polymerization in fusing myoblasts (reviewed in Haralalka and Abmayr [2010]). In the pupal eye, our fluorescence-based imaging did not provide sufficient resolution to assess whether similar aggregation of Rac occurred in IPC cellular extensions: we observed a mild, though not significant, enhancement of *GMR>dArf6*^{RNAi} mispatterning in a Rac$^{+/-}$ heterozygous background (Figure 6, A, B, and D, and Table S3). In addition, *GMR>dArf6*^{RNAi} was also dominantly modified by *Rho1* (Figure 6, C and D, and Table S3), which linked two small GTPases to dArf6-mediated actin dynamics.

To assess whether Arf6 has a more general role in actin dynamics and cell placement within epithelia, we manipulated dArf6 activity in cells that generate the central region of the adult notum cuticle. During pupal metamorphosis, sheets of epithelial cells migrate toward the midline to seal the thorax (Zeitlinger and Bohmann, 1999). Disrupted migration leads to aberrations in the adult notum cuticle structure. We observed a similar disruption when ArfGAP, ArfGEF, or Arf6 levels were altered (Figure S5).

We also observed differences in the organization of actin at the level of individual cells. In control eyes, phalloidin staining revealed an intricate web of apical actin filaments and bundles that became increasingly organized during pupal development. At 23 h APF, F-actin tracked along cellular AJs and numerous short filaments or bundles filled the apical cytoplasm (Figure 6E, red arrow). By 27 h APF, the density of phalloidin increased and polarized F-actin bundles traversed IPCs (Figure 6F, red arrow). A dense "bush" of actin radiated from the central four cone cells, and numerous bundles filled the cytoplasm of 1°s (Figure 6F). By 41 h APF, the F-actin in 1°s was oriented to extend across the width of each cell (Figure 6G, green arrow); in IPCs F-actin bundles were oriented along the length of each cell (Figure 6G). When we strongly perturbed dArf6, phalloidin staining revealed fewer clearly defined cytoplasmic actin filaments or bundles at 23 h APF (Figure 6H, red arrow). Phalloidin staining of actin was weaker at 27 h APF compared with wild-type tissue, and F-actin bundles in IPCs were shorter and less well polarized (Figure 6I, red arrow). At 41 h APF, F-actin bundles were short and organized neither across the width of 1°s (Figure 6J, green arrow) nor along the lengths of IPCs. Further, the dense actin staining around the circumference of 1° cells adjoining IPCs, as well as

FIGURE 5: *dArf6* interacts with *ArfGAP* and *ArfGEF* loci. *dArf6*^{RNAi} patterning defects (A) were enhanced in eyes heterozygous for (B) *dArfGAP3*^{e01250}, (C) *dAsap*^{KG03963}, (D) *siz*^{T1032}, and (E) *dPsd*$^{KO\#1}$. In all right-hand panels, IPCs are pseudocolored green, and several characteristic patterning errors are highlighted as described in Figure 2. All tissue was dissected at 41 h APF; α-DE-cadherin labels AJs. (F) Graph of the mean number of patterning errors (OMS) observed in these genetic interactions. Error bars represent SE. Refer to Table S3 for detailed analyses. Scale bars: 10 μm.

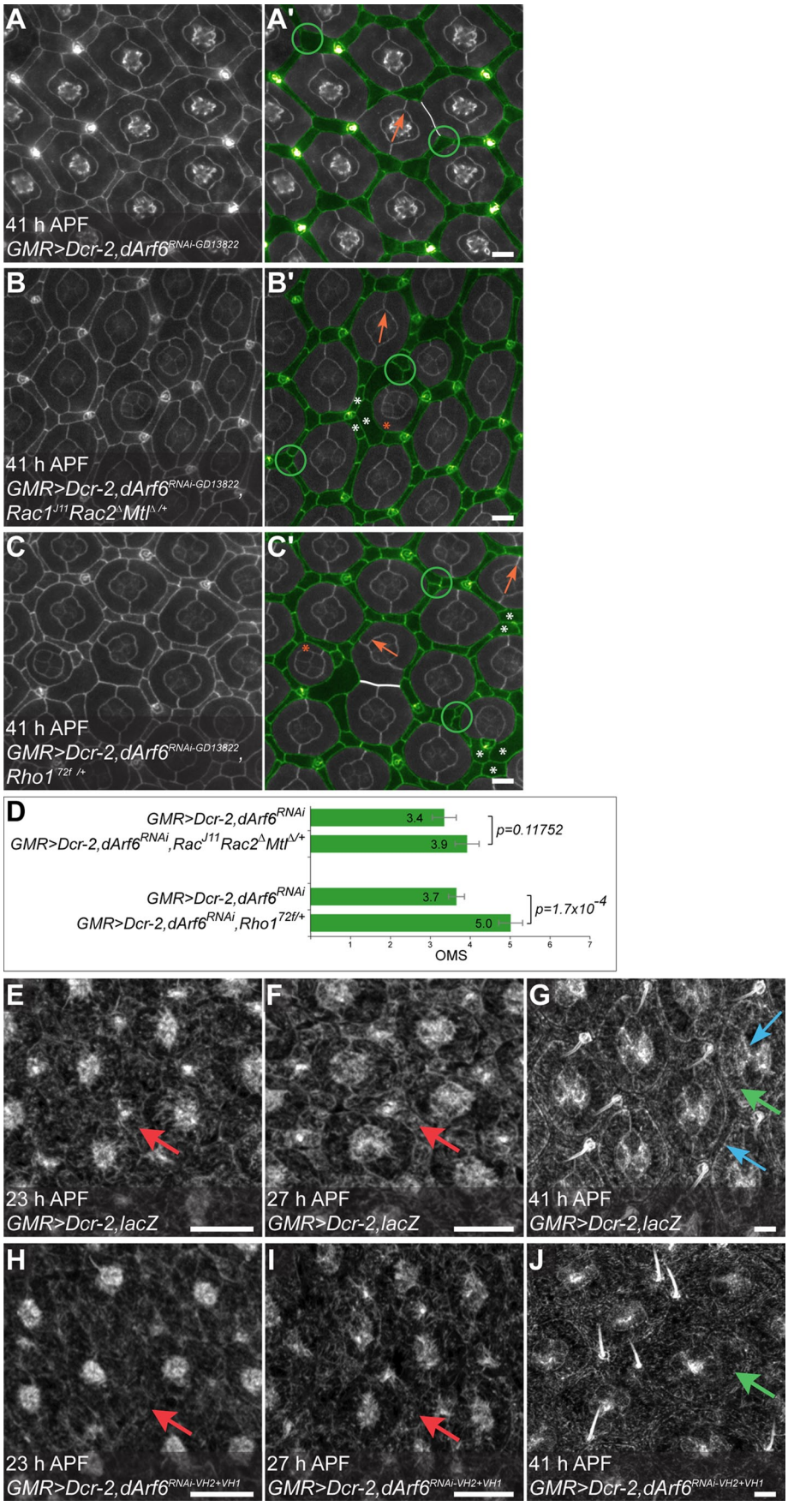

FIGURE 6: Evidence for *dArf6* regulation of actin. (A) The *dArf6*^{RNAi} phenotype was enhanced in (B) *Rac* or (C) *Rho1* heterozygotes. Eye tissue was dissected at 41 h APF; α-DE-cadherin labels AJs. IPCs are pseudocolored green, and examples of characteristic patterning errors are highlighted as described in Figure 2. Interactions are graphed in (D) and shown in detail in Table S3. The interaction with Rac was not statistically significant. Error bars reflect SE. (E–J) Phalloidin staining revealed an intricate apical mesh of F-actin filaments. (E, F, and G) In control tissue, F-actin tracks cell boundaries, fills the apical profile, and polarizes with development. (H, I, and J) When *dArf6* is greatly decreased, weaker phalloidin staining reveals a less well-organized cytoskeleton. Red arrows indicate F-actin strands in IPCs (E, F, H, and I), green arrows indicate F-actin in 1°s (G and J), blue arrows indicate F-actin accumulation at 1° or cone cell boundaries. Scale bars: 10 μm.

along the boundaries of cone cells, was abolished in *dArf6*^{RNAi} tissue (Figure 6G, blue arrows, compare with 6J). These data demonstrate an important role for dArf6 in actin polymerization and organization in the developing pupal eye.

Together with our in situ movies (Movies S2–S4), these data strongly support a role for dArf6 in situ in remodeling the complex actin cytoskeleton and actin-rich structures in cells as they move within the epithelium.

dArfGAP3 and dAsap directly bind the adaptor protein Cindr

We previously described a role for the adaptor protein Cindr in regulating actin-dependent cell movements in the pupal eye (Johnson *et al.*, 2008). Reducing Cindr lead to ectopic movement of IPCs in the retinal field (Movie S5). Cindr mediates these effects in part through a direct interaction with the capping proteins Cpa and Cpb. However, *cindr* hypomorphic eyes are more severely mispatterned than *cpa* or *cpb* mutants (Johnson *et al.*, 2008; unpublished data). This suggests that multiple pathways function downstream of Cindr to regulate actin dynamics. Consistent with this view, our coimmunoprecipitation studies identified dArfGAP3 as a novel interaction partner of the tagged isoform Cindr^{TAP} (Figure 7A). In vitro dArfGAP3 bound mostly to the C-terminal fragment of Cindr distal to the three conserved N-terminal Src homology 3 (SH3) domains (Figures 7A and S3A). Similarly, we identified dAsap as bound to Cindr (Figure 7B).

These data suggest that both dArfGAP3 and dAsap associate with the cell surface through direct interactions with Cindr; in fact, we observed partial colocalization between these proteins in vivo (unpublished data). Previous work indicated that the mammalian ASAP bound to the SH3 domains of the Cindr orthologue CIN85 (Kowanetz *et al.*, 2004; Liu *et al.*, 2005).

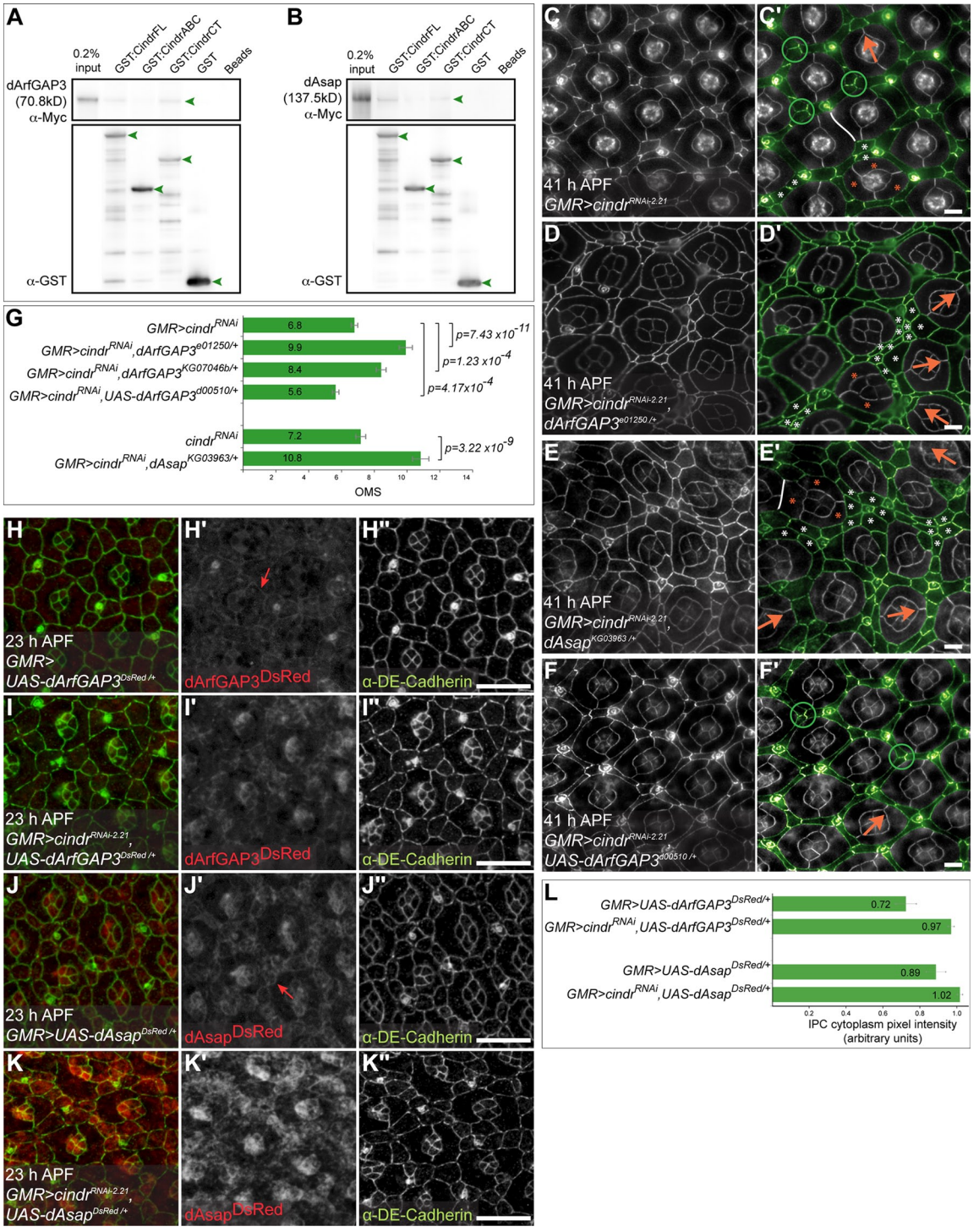

FIGURE 7: dArfGAP3 and dAsap bind Cindr to form a complex essential for eye patterning. GST-binding assays confirmed binding between (A) dArfGAP3 and (B) dAsap and full-length Cindr (GST:CindrFL, 122 kDa), as well as the shorter CindrCT (83 kDa). A small amount of both dArfGAP3 and dAsap bound the three SH3 domains of Cindr (CindrABC, 62 kDa). Green arrowheads relate to relevant full-length fragments. Blots were probed with α-Myc (top) or α-GST (bottom). (C) The pupal eye was mispatterned when a mild RNAi transgene targeting *cindr* was expressed. When one copy of either (D) *dArfGAP3* or (E) *dAsap* was removed, *GMR>cindr*^{RNAi} mispatterning was severely enhanced. These phenotypes are virtually indistinguishable. (F) Overexpressing *dArfGAP3* suppressed *cindr*^{RNAi}. (G) Graph of OMS values of these genetic interactions; highly significant p values and SEs are indicated. Refer to Table S4 for detailed analyses. (H–L) Reducing *cindr* expression impaired recruitment of ArfGAPs to the membrane. (H and J) Ectopic dArfGAP3 and dAsap (H′ and J′) localized evenly at the AJs of wild-type retinal cells (red arrows). (I and J) In *cindr*^{RNAi} retina, AJs were perturbed (as described previously [Johnson *et al.*, 2008]), membrane localization of dArfGAP3 and dAsap was disrupted, and cytoplasmic levels increased. This was confirmed by quantification of the pixel intensity of ArfGAP3^{DsRed} and Asap^{DsRed} fluorescence in the cytoplasm of IPCs. (L) Eyes were dissected at times indicated; α-DE-cadherin labels AJs. IPCs are pseudocolored green in (C–F), and characteristic patterning errors are highlighted as in Figure 2. Scale bars: 10 μm.

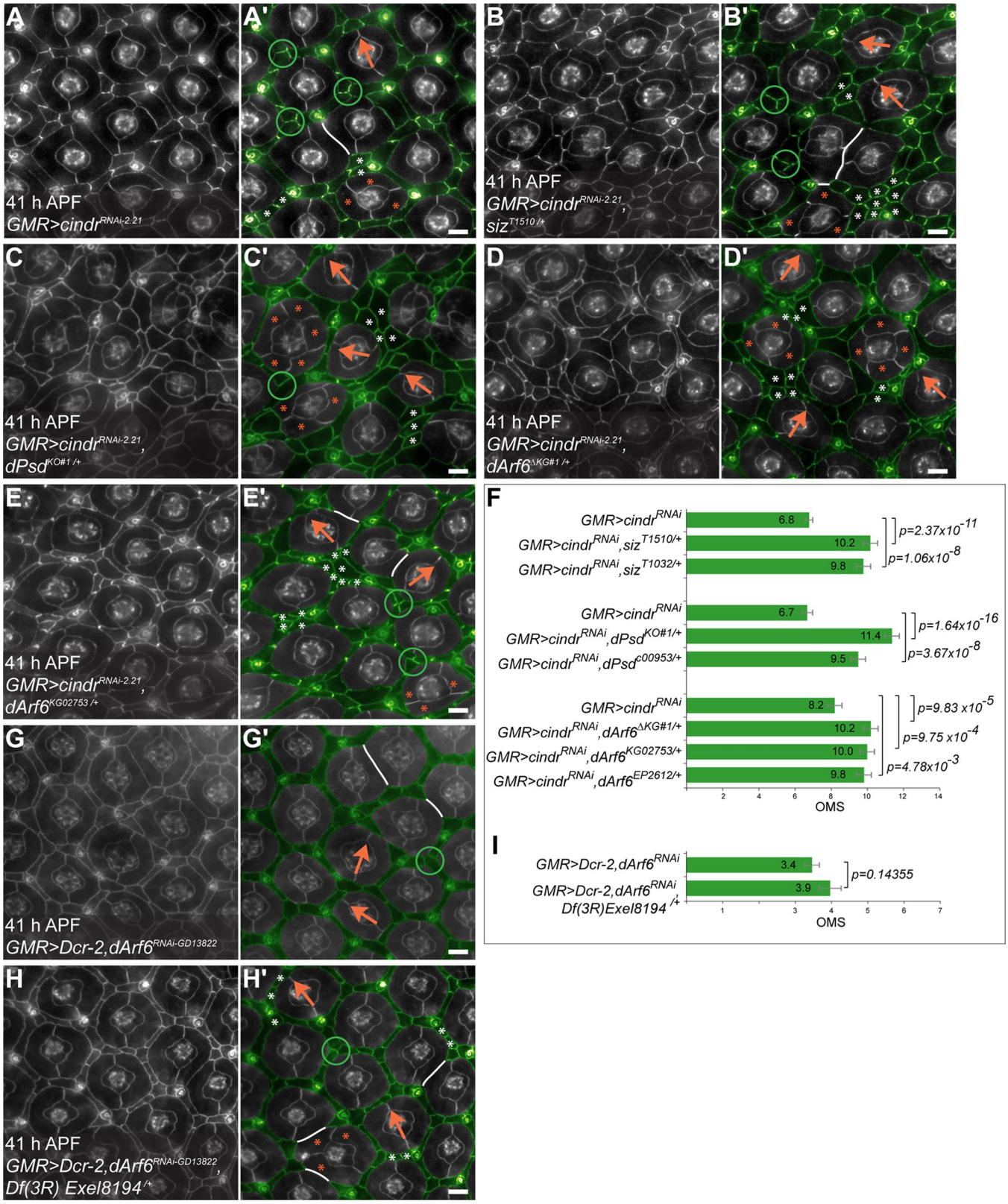

FIGURE 8: *cindr*^{RNAi} is modified by the ArfGEFs and Arf6. (A) *GMR>cindr*^{RNAi} patterning defects were enhanced by (B) *siz*^{T1510}, (C) *dPsd*$^{KO\#1}$, and (D) *dArf6*$^{KG\#1}$ null alleles and (E) *dArf6*^{KG02753}. (F) Graph of OMS values for these interactions and additional alleles; p values and SEs are indicated. Refer to Table S4 for detailed analyses and statistics. *dArf6*^{RNAi} mispatterning (G) was enhanced by the *Df(3R)Exel8194* deficiency (H), which removes *cindr*. This interaction, shown in (I), is not statistically significant. See Table S4 for further analyses. All tissue was dissected at 41 h APF; α-DE-cadherin labels AJs; characteristic patterning errors are highlighted as in Figure 2. Scale bars: 10 μm.

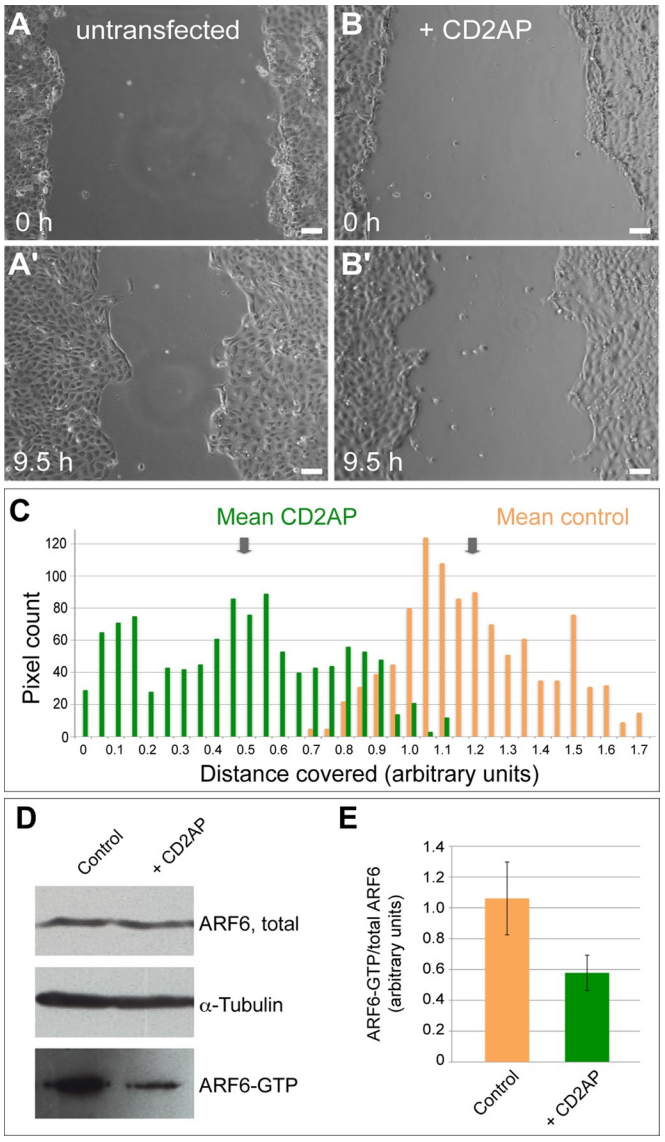

FIGURE 9: The Cindr-Arf6 interaction is conserved. (A–D) Confluent monolayers of Madin-Darby canine kidney (MDCK) cells were cleared ("wounded") and ARF6^{GTP} levels were examined at 0- and 10-h postwounding. (A) Recovery of untransfected cells at time 0 h (top) and 9.5 h (bottom) after scratch injury. (B) An example of migrating MDCK cells transfected with the Cindr orthologue CD2AP at 0 and 9.5 h after wounding. The distance covered is presented graphically in (C). (D) Active ARF6^{GTP} levels were reduced in migrating MDCK cells expressing ectopic CD2AP (right lane) when compared with untransfected migrating cells (left lane). (E) Band density was measured by densitometry and the ratios of ARF6^{GTP} to total ARF6 are shown. Values are the mean of three separate experiments ± SD. Scale bars: 100 μm.

Surprisingly, although *Drosophila* dAsap also contains a conserved CIN85 interaction motif (Kowanetz *et al.*, 2004; Liu *et al.*, 2005), it interacted mainly with the C-terminal fragment CindrCT (Figures 7B and S3A).

To further validate the in situ importance of direct Cindr:ArfGAP interactions, we tested for functional interactions between the two loci during IPC patterning. We previously reported that reducing *cindr* activity (*GMR>cindr^{RNAi}*) led to multiple errors in the final arrangement of cells (Figure 7C and Table S4; Johnson *et al.*, 2008). These patterning errors were strongly increased when a functional genomic copy of either *dArfGAP3* or *dAsap* was removed (Figure 7, D, E, and G, and Table S4). These statistically significant dominant genetic interactions were characterized by a large number of additional IPCs that contributed to a decline in the ordered arrangement of the lattice: few 2° or 3° niches were correctly specified and the hexagonal shape of most ommatidial facets was distorted (Figure 7, D and E). Primary pigment cell and cone cell errors also increased, and misorientation of ommatidia became more pronounced. In contrast, overexpressing *dArfGAP3* (*GMR>UAS-dArfGAP3^{d00510}*) partially suppressed *cindr^{RNAi}*-mediated mispatterning (Figure 7, F and G, and Table S4). Of note, ectopic expression of *dArfGAP3^{DsRed}* (expressed at lower levels [unpublished data]) and *dAsap^{DsRed}* transgenes led to mild patterning defects (Figure S3, K and L). These transgenes may have dominant-negative or alternative functions: their expression enhanced *cindr^{RNAi}* mispatterning in the same manner as several *dArfGAP3* and *dAsap* alleles (Figure S6, A–C, and Table S4).

We hypothesized that Cindr may facilitate the role of the ArfGAPs by recruiting them to the plasma membrane and to sites of actin regulation during IPC patterning. We tested this view by depleting Cindr protein. Strongly depleting *cindr* led to severely disrupted cell morphology, and ArfGAP localization became difficult to accurately assess. Weakly reducing *cindr* elevated cytoplasmic levels of both endogenous and ectopic dAsap and dArfGAP3^{RFP}, although AJ localization was still observed (Figure 7, H–L; unpublished data). In contrast, dPsd^{GFP} did not change when Cindr was reduced (unpublished data), although these two proteins also colocalized in vivo (Figure 4D).

Functional interactions between Cindr and dArf6, Siz, and dPsd

Genetic interactions between *cindr^{RNAi}* and multiple alleles of *siz*, *dPsd*, and *dArf6* support the view that the Arf regulatory cycle depends on Cindr during IPC patterning. In each case, removing one genomic copy of these loci strongly enhanced *cindr^{RNAi}* mispatterning (Figure 8, A–F, and Table S4). These phenotypes were strikingly similar to those observed in genetic interactions between *cindr* and the ArfGAPs (compare with Figure 7, C–G): again IPC patterning was most severely disrupted. Similarly, *dArf6^{RNAi}* patterning was mildly enhanced in a background heterozygous for *Df(3R)Exel8194*, a deficiency that includes *cindr* (Figure 8, G–I, and Table S3). The interaction did not achieve statistical significance, perhaps because this large deficiency contained other modifiers of *dArf6^{RNAi}*.

Taken together, our data support a model in which Cindr binds ArfGAP-class proteins in order to regulate Arf6 activity; this in turn regulates the ability of cells to move into new niches within the emerging epithelium. We next explored a standard mammalian cell migration assay to determine whether this Cindr/Arf6 activity is conserved. Utilizing a scratch assay, we observed reduced migration of MDCK cells that expressed ectopic CD2AP (Figure 9, A–C): the CD2AP-transfected cell populations migrated more slowly than mock-transfected controls. Decreased migration was accompanied by reduced Arf6 activity (Figure 9, D and E); interestingly, Arf6-GTP levels were unaffected by CD2AP expression when cells were quiescent (unpublished data). Unfortunately, attempts to reduce ASAP and ArfGAP3 proved toxic to cells. Nevertheless these data emphasize the requirement for Cindr/CD2AP in regulating Arf6 during cell motility.

dArf1 and dArf6 have different roles in eye development

In addition to targeting Arf6, mammalian orthologues of dArfGAP3 and dAsap can also target Arf1, which localizes predominantly to Golgi and endoplasmic reticulum (ER) membranes (Gillingham and Munro, 2007; Randazzo *et al.*, 2007). We therefore examined the

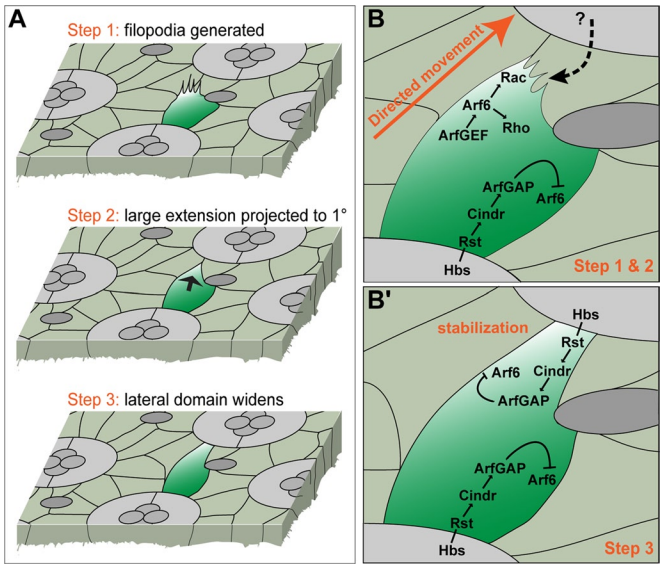

FIGURE 10: Model of directed cell movement. (A) A schematized view of cell movements based on a movie of a wild-type eye region. Cell intercalation begins with the extension of numerous filopodia (step 1). These extend to generate a large cellular extension (step 2) toward a target ommatidium. Once the extension reaches the ommatidium, it extends laterally, and the cell securely occupies the entire niche (step 3). (B and B′) One potential model for the molecular and spatial events that guide a cell into a new niche. A signal—perhaps mediated through EGFR—recruits ArfGEFs to the membrane to activate dArf6. Downstream of this signal 1) Rac is activated to generate extending filopodia and 2) Rho induces contraction of the actin–myosin cytoskeleton to coordinate changes in the cell's shape. Eventually, 3) *trans* binding of the surface protein Rst to Hbs recruits Cindr/ArfGAP complexes to the membrane to 4) inhibit dArf6 activation and 5) stabilize the cytoskeleton and AJs at the local plasma membrane. Other models that emphasize more directed signals are also possible.

role of dArf1 (Arf79F) in patterning the pupal eye. Unlike dArf6, ectopic dArf1^{myc} localized to regions occupied by the Golgi and ER and not to the cell membrane or regions of actin remodeling (Figure S7A). Though both led to failure to correctly establish 3°s, reducing *dArf1* failed to generate several phenotypes characteristic of *dArf6*^{RNAi}, including multiple rows of IPCs, fusion of neighboring ommatidia, ectopic 1°s, and misrotated ommatidium (Figure S7B). Further, *dArf1*^{RNAi} expression resulted in unevenly distributed DE-cadherin (Figure S7, B and C) and, as pupal eye tissue matured (by 41 h APF), large apical gaps formed as 1°s "unclasped" and retracted from previously encircled ommatidia and IPCs withdrew from neighboring 1°s. Remarkably, the retracted cells did not appear apoptotic immediately after losing AJ-mediated adhesion. This unusual in vivo phenotype has not to our knowledge been previously reported; the mechanism by which dArf1 maintains stable AJs warrants further study.

We observed complex genetic modifier interactions between dArf1 and Cindr that did not rise to the level of statistical significance (Table S4 and Figure S7, D–G); also, *dArf1*^{RNAi} defects were not modified in *dArfGAP3* or *dAsap* heterozygotes (unpublished data). We conclude that Cindr likely regulates dArf1 and dArf6 in independent processes.

DISCUSSION

In this study, we have taken advantage of *Drosophila* to explore the in situ details of Arf6 and patterning. Directed knockdown combined with time-lapse microscopy revealed important changes in cell behavior in emerging eye epithelia when Arf6 or Cindr were compromised. In wild-type retina, we observed large cellular extensions that catalyzed successful cell intercalations as IPCs moved to inhabit new niches (Figure 1 and Movie S1). These cell projections extended first from the apical domains of IPCs and then basally once secure AJs were generated (Figure 1B; unpublished data). These directed cell extensions were aberrant in *dArf6*^{RNAi} or *cindr*^{RNAi} tissue and led to reduced or ectopic cell movement, respectively, that then disrupted cell intercalation (Figure 1 and Movies S2–S5). This then inhibited the generation of a stereotyped pattern of IPC arrangement (Figures 2, B–E, and 7C).

A model for directional IPC movement

Our model combines molecular and spatial information to propose a mechanism that guides these cellular extensions, which in turn direct successful cell intercalation and stabilization. This potential model is presented in Figure 10. In this view, Rst/Hbs complexes recruit Cindr to the surface, which recruits the ArfGAPs dArfGAP3 and dAsap to locally reduce dArf6 activity. Other regions within the IPC are free to activate dArf6—either spontaneously or by signals such as epidermal growth factor receptor (EGFR; Freeman, 1996; Miller and Cagan, 1998)—through the ArfGEFs Siz and dPsd. Locally activated dArf6 in turn amplifies Rac-induced actin polymerization and Rho-induced contractile forces to promote cellular extensions. As an IPC's extension contacts a 1°, Rst (within the IPC) and Hbs (within the 1°) are stabilized at the site of contact, suppressing dArf6 and establishing the cell's new position within the epithelium (Figure 10, A and B). Junctions are later established, settling the local pattern.

This model accounts for directional generation of cell extensions away from stable IPC:1° boundaries, as well as the stabilization of new IPC:1° boundaries that then widen laterally. In addition, it accounts for gradual accumulation of Cindr, dAsap, and dArfGAP at AJs, as IPCs stabilize and the eye matures (Figure S3; Johnson *et al.*, 2008).

Arf6 regulates cell extensions and is restricted by Cindr

Are all cell extensions dependent on dArf6? Partial loss-of-function *dArf6*^{RNAi} IPCs generated multiple, small, cell extensions that were rapidly and frequently withdrawn (Movies S2–S4). This suggests that either a small amount of dArf6 activity permits small, poorly effective extensions or that cells have an independent ability to generate small extensions and dArf6 activity promotes the much larger extension required for directed cell movement. In the latter view, dArf6 activity locally amplifies Rac, Rho, and perhaps other activators of actin polymerization. We propose that this activity is spatially restricted by Cindr. Consistent with this view, *cindr*$^{-}$ IPCs were hypermotile; they successfully generated cellular extensions and moved into proper niches but typically failed to stabilize within the niche and instead often moved away (Movie S5; Johnson *et al.*, 2008). Conversely, in mammalian cells expressing ectopic CD2AP, Arf6 activity and motility were reduced (Figure 9, A–E).

Several lines of evidence support our model. Reducing activity of *cindr*, *dArfGAP3*, *dAsap*, *siz*, *dPsd*, or *dArf6* led to similar patterning defects; further, the proteins colocalized and the loci demonstrated functional genetic interactions. Reducing *cindr* enhanced cell motility (Movie S5; Johnson *et al.*, 2008), while reducing *rst* or *dArf6* hampered intercalation (Movies S2–S4; Larson *et al.*, 2008). Coupled with preferential adhesion between 1°s and IPCs (Bao and Cagan, 2005), this model provides a mechanism for the coordination of surface interactions and cytoskeletal changes (Figure 10B).

The Cindr:ArfGAP:dArf6 regulatory cassette described here is likely conserved in other tissues and across species, both during

development and to maintain homeostasis. Indeed, extensive data have linked multiple mammalian ArfGAPs, including GEP100 and Arf6, to metastatic cell invasion (reviewed by Ha *et al*. [2008]; Premont and Schmalzigaug [2009]; Sabe *et al*. [2009]). The Cindr orthologue CIN85 has been implicated in ASAP1-induced invasion in culture, leading to the view that CIN85 mediates ASAP monoubiquitination by the E3 ligase Cbl to promote invasion (Nam *et al*., 2007). Our work provides a template to consider the interactions of these factors in mediating surface events and guiding cells into unique sites within emerging epithelial.

MATERIALS AND METHODS

Fly stocks

The following fly stocks (from the Bloomington Drosophila Stock Center [BDSC; Bloomington, Indiana], Vienna Drosophila RNAi Center [VDRC; Vienna, Austria], National Institute of Genetics [NIG; Shizuoka, Japan], Elizabeth Chen [Johns Hopkins University School of Medicine], Yang Hong [University of Pittsburgh School of Medicine], and Patricio Olguin [Mount Sinai School of Medicine]) were used:

Transgenic RNAi lines: *UAS-cindr*$^{RNAi\text{-}2.21}$ (Johnson *et al*., 2008); *UAS-dArfGAP3*$^{RNAi\text{-}GD12053}$ that was mobilized using standard techniques to generate *UAS-dArfGAP3*$^{RNAi\text{-}VH1}$ and *UAS-dArfGAP3*$^{RNAi\text{-}JF01649}$; *UAS-dAsap*$^{RNAi\text{-}GD8897}$ that was mobilized to generate *UAS-dAsap*$^{RNAi\text{-}VH7a+VH7b}$, *UAS-dAsap*$^{RNAi\text{-}KK102760}$, *UAS-dAsap*$^{RNAi\text{-}JF01626}$, *UAS-siz*$^{RNAi\text{-}GD14895\text{-}v36625}$, *UAS-siz*$^{RNAi\text{-}GD14895\text{-}v36627}$, *UAS-dPsd*$^{RNAi\text{-}GD14945}$, and *UAS-dPsd*$^{RNAi\text{-}31158R\text{-}2}$; *UAS-dArf6*$^{RNAi\text{-}GD13822}$ that was mobilized to generate the two-insert line *UAS-dArf6*$^{RNAi\text{-}VH2+VH1}$, *UAS-dArf6*$^{RNAi\text{-}JF02454}$, *UAS-dArf6*$^{RNAi\text{-}KK108126}$, and *UAS-dArf1*$^{RNAi\text{-}GD12522}$.

Driver lines: *GMR-GAL4* (on X or II), *tubulin-GAL4*, *ptc-GAL4*, and *Pnr-GAL4* (Calleja *et al*., 1996).

Alleles: *dArfGAP3*^{e01250}, *dArfGAP3*^{KG07046b} (an additional insertion on chromosome II was removed), *dArfGAP3*^{d00510} (includes UAS sites), *dAsap*^{KG03963}, *siz*^{T1510}, *dArf6*^{KG02753}, *dArf6*^{EP2612}, *dArf1*^{EY00996}, *dArf1*^{EY08473}, *Df(3R)Exel8194*, *rst*^{3}, *hbs*^{459}, *Rac1*^{J11}, *Rac2Δ Mtl*Δ *Rho1*^{72f}, *dPsd*^{c00953}, *dPsd*$^{KO\#1}$, *dPsd::GFP-C*, *dArf6ΔKG#1*, and *dArf6::GFP-C* (Huang *et al*., 2009).

UAS expression constructs: *UAS-dArfGAP3*^{DsRed}, *UAS-dAsap*^{DsRed}, *UAS-dArf6*^{myc}, and *UAS-dArf1*^{myc} are described in the section *Transgenic expression lines*; *UAS-dArf6*^{DN} (Chen *et al*., 2003), *UAS-Dcr-2*, and *UAS-lacZ*.

For genetic interactions: 1) *GMR-GAL4*; *UAS-cindr*$^{RNAi\text{-}2}$*/SM6a-TM6B* virgins or 2) *GMR-GAL4*, *UAS-Dcr-2*; *UAS-dArf6*$^{RNAi\text{-}GD13822}$ virgins were crossed to the allele or transgene of interest and for controls to *w*^{1118} or *UAS-lacZ*, as appropriate. To test interactions between *dArf6*$^{RNAi\text{-}GD13822}$ and *rst*^{3} (located on X chromosome), females were dissected. For all other genetic interactions, males only were dissected.

Imaging and phenotypic analysis

Pupae were gathered at 0 h APF and dissected as described (Bao and Cagan, 2005). Transmission electron micrographs (TEMs) were prepared as previously described (Cagan and Ready, 1989). For immunochemistry, primary antibodies were rabbit anti-Cindr (1:100; Johnson *et al*., 2008), rat anti–DE-Cad2 (1:20; DSHB, Iowa City, Iowa), rabbit anti-dAsap (1:20), guinea-pig anti-dArfGAP3 (1:20), and rabbit anti–cleaved caspase 3 (1:200; Cell Signaling Technology, Danvers, MA). To visualize F-actin, rhodamine-phalloidin was included in primary antibodies incubations (1:100; Invitrogen, Carlsbad, CA). Secondary antibodies were conjugated to Cy5 (Jackson ImmunoResearch Laboratories, West Grove, PA) or Alexa Fluor 488 or 568 (Invitrogen). Samples were mounted in 0.5% n-propylgallate in 80% glycerol. Confocal or fluorescence images were gathered using Leica Microsystems TCS SP5 DM or DMI microscopes (Leica Microsystems, Chicago, IL). Images were minimally processed and pseudocolor was introduced in Photoshop (Adobe, San Jose, CA).

Phenotypic analysis was performed as previously described (Johnson and Cagan, 2009). Briefly, images of the apical profile were divided into hexagonal fields by connecting the center of six ommatidia surrounding a central ommatidium. Each hexagonal field was one data point, and all patterning errors observed within each data point were totaled. A mean OMS was calculated as the average number of errors scored within 75 data points of each genotype. Student's *t* test was used to determine p values and statistical significance. OMS values, together with complete analyses of patterning errors observed and total interommatidial cell number, are provided in Tables S1, S3, and S4.

MetaMorph (MDS Analytical Technologies, Sunnyvale, CA) was utilized to measure the pixel intensity of fluorescent ArfGAP3^{DsRed} and Asap^{DsRed} in a standard cytoplasmic region of 40 IPCs randomly selected from at least three different images. Mean values are graphed (Figure 7L); units are arbitrary.

For live imaging, movies of 1) *GMR-Gal4, UAS-Dcr-2/Y*; *UAS-lacZ/UAS-α-Catenin*^{GFP}; 2) *GMR-Gal4, UAS-Dcr-2/Y*; *UAS-dArf6*$^{RNAi\text{-}GD13822}$*/UAS-α-Catenin*^{GFP}; and 3) *GMR-Gal4, UAS-α-Catenin*^{GFP}*/ +*; *UAS-cindr*$^{RNAi\text{-}2.21}$ pupae were generated as previously described (Larson *et al*., 2008). Pseudocolor and annotations were introduced in Photoshop.

Quantitative PCR analysis of RNAi transgenes

mRNA was prepared from 10 whole wandering L3 larvae of each genotype (*tubulin-GAL4>UAS-geneX*^{RNAi}) using standard Trizol extraction. For pupal eye preparations, mRNA was extracted from eyes dissected from 28 to 30 pupae staged to 40–41 h APF (genotype: *GMR-GAL4>UAS-Dcr-2,UAS-geneX*^{RNAi}). qPCR was performed with the ABI PRISM 7900HT (Mount Sinai School of Medicine qPCR Shared Resource Facility). Primers are listed in Table S5.

Transgenic expression lines

Full-length dAsap cDNA was PCR-amplified from clone RH04774 (Drosophila Genomics Resource Center, Bloomington, IN) introducing *Kpn* and *Not*I; full-length dArfGAP3 was amplified from LD46935 introducing *Eco*RI and *Xho*I sites. These were ligated into pUAST-DsRed(C-T) (Seppa *et al*., 2008). Arf6 and Arf1 were amplified from clones RE16882 and LD24904, introducing *Bgl*II/*Xho* and *Eco*RI/*Xho* sites, respectively, and ligated into pUAST-HM (Parker *et al*., 2001). Transgenic flies were generated using standard techniques (BestGene, Chino Hills, CA).

dAsap and dArfGAP antibodies

We generated polyclonal guinea-pig antibodies against a fragment of dArfGAP3 (amino acids 134–355) and polyclonal rabbit antibodies for dAsap (amino acids 754–1092) with assistance from Covance (Princeton, NJ) and Proteintech Group (Chicago, IL), respectively, using standard procedures.

Binding assays

The glutathione *S*-transferase (GST):Cindr fusion proteins were generated by cloning full-length Cindr (645–3294 base pairs), the three SH3 domains (CindrABC, 645–1677 base pairs), or the N-terminal SH3 domains (CindrCT, 1680–3294 base pairs) into *Bam*HI/*Xho*I of pGEX-4T. Fusion proteins were raised and isolated from BL-21 cells. Full-length dAsap and dArfGAP3 cDNA were PCR-amplified from RH04774 and LD46935, introducing *Eco*RI/*Xho*I and *Avr*II/*Avr*II sites,

respectively, for ligation into pCS2+MT (gift from S. Sokol, Mount Sinai School of Medicine). Myc-tagged protein products were generated with the TnT Quick Coupled Transcription/Translation System (Promega, Madison, WI). Translated products were divided equally among aliquots of GST:CindrFL (122 kDa), CindrCT (83 kDa), CindrABC (62 kDa), GST, and glutathione beads only. Binding assays were performed using standard protocols and analyzed on NuPage 4–12% gradient SDS–PAGE (Invitrogen) and mouse anti-Myc (1:1000; Cell Signaling) and rabbit anti-GST (1:1000; Santa Cruz Biotechnology, Santa Cruz, CA).

Scratch-wound assays

Approximately 6×10^5 MDCKI cells were plated per well of a six-well tissue culture plate, grown overnight, and transfected with pCMV6-AC-CD2AP-GFP (Origene, Rockville, MD) or a control plasmid. At 24 h posttransfection, cells were "wounded" with a p10 micropipettor tip, washed in serum-free media, and imaged (t = 0) with a Zeiss (Carl Zeiss Microimaging, Thornwood, NY) Axiobserver Z1 microscope. To calculate the distance cells traveled during healing, the wound edges were first mapped in images at times t = 0 and t = 9.5 h. These edge maps were saved as a series of coordinate pairs [(x_1, y_1); (x_2, y_2); (x_3, y_3)…(x_n, y_n)], the Euclidean distance was calculated on a point-by-point basis, and the results were plotted in a histogram. The data shown are representative of three independent experiments.

ARF6 activity assay

At 0- and 10-h postwounding, MDCKI cells were lysed, and equivalent amounts of protein lysate were examined for ARF6-GTP levels using a previously described pulldown assay (Schweitzer and D'Souza-Schorey, 2002). Cell lysates were separated by Western blot analysis and probed for total Arf6 and for α-tubulin as a loading control. Band density was measured by densitometry to determine the ratios of ARF6-GTP to total ARF6.

ACKNOWLEDGMENTS

We thank BDSC, VDRC, NIG, Elizabeth Chen, Yang Hong, and Patricio Olguin for fly lines; Sergei Sokol for the pCS2+MT vector; Erdem Bangi, Jay Pendse, and Vivek Rudrapatna for comments on the manuscript; and James Clancy and Vandhana Chari for assistance and advice on the scratch-wound assays. This work was funded by RO1 EY1149 and RO1 CA115316. In addition, we thank the staff of the MSSM Shared Resource Facility (supported by NIH-NCI shared resources grant 5R24 CA095823-04, NSF Major Research Instrumentation grant DBI-9724504, and NIH shared instrumentation grant 1 S10 RR0 9145-01) and the MSSM qPCR Shared Resource Facility for assistance.

REFERENCES

Aman A, Piotrowski T (2009). Cell migration during morphogenesis. Dev Biol 341, 20–33.

Bao S, Cagan R (2005). Preferential adhesion mediated by Hibris and Roughest regulates morphogenesis and patterning in the *Drosophila* eye. Dev Cell 8, 925–935.

Cagan R (2009). Principles of *Drosophila* eye differentiation. Curr Top Dev Biol 89, 115–135.

Cagan RL, Ready DF (1989). The emergence of order in the *Drosophila* pupal retina. Dev Biol 136, 346–362.

Calleja M, Moreno E, Pelaz S, Morata G (1996). Visualization of gene expression in living adult *Drosophila*. Science 274, 252–255.

Chen EH, Pryce BA, Tzeng JA, Gonzalez GA, Olson EN (2003). Control of myoblast fusion by a guanine nucleotide exchange factor, loner, and its effector ARF6. Cell 114, 751–762.

Claing A (2004). Regulation of G protein-coupled receptor endocytosis by ARF6 GTP-binding proteins. Biochem Cell Biol 82, 610–617.

Donaldson JG (2003). Multiple roles for Arf6: sorting, structuring, and signaling at the plasma membrane. J Biol Chem 278, 41573–41576.

Donaldson JG, Honda A (2005). Localization and function of Arf family GTPases. Biochem Soc Trans 33, 639–642.

D'Souza-Schorey C, Chavrier P (2006). ARF proteins: roles in membrane traffic and beyond. Nat Rev Mol Cell Biol 7, 347–358.

Freeman M (1996). Reiterative use of the EGF receptor triggers differentiation of all cell types in the Drosophila eye. Cell 87, 651–660.

Gillingham AK, Munro S (2007). The small G proteins of the Arf family and their regulators. Annu Rev Cell Dev Biol 23, 579–611.

Ha VL, Luo R, Nie Z, Randazzo PA (2008). Contribution of AZAP-Type Arf GAPs to cancer cell migration and invasion. Adv Cancer Res 101, 1–28.

Haralalka S, Abmayr SM (2010). Myoblast fusion in *Drosophila*. Exp Cell Res 316, 3007–3013.

Huang J, Zhou W, Dong W, Watson AM, Hong Y (2009). Directed, efficient, and versatile modifications of the *Drosophila* genome by genomic engineering. Proc Natl Acad Sci USA 106, 8284–8289.

Jaworski J (2007). ARF6 in the nervous system. Eur J Cell Biol 86, 513–524.

Johnson RI, Cagan RL (2009). A quantitative method to analyze Drosophila pupal eye patterning. PLoS One 4, e7008.

Johnson RI, Seppa MJ, Cagan RL (2008). The *Drosophila* CD2AP/CIN85 orthologue Cindr regulates junctions and cytoskeleton dynamics during tissue patterning. J Cell Biol 180, 1191–1204.

Kowanetz K *et al*. (2004). CIN85 associates with multiple effectors controlling intracellular trafficking of epidermal growth factor receptors. Mol Biol Cell 15, 3155–3166.

Larson DE, Liberman Z, Cagan RL (2008). Cellular behavior in the developing *Drosophila* pupal retina. Mech Dev 125, 223–232.

Le Clainche C, Carlier MF (2008). Regulation of actin assembly associated with protrusion and adhesion in cell migration. Physiol Rev 88, 489–513.

Liu Y, Yerushalmi GM, Grigera PR, Parsons JT (2005). Mislocalization or reduced expression of Arf GTPase-activating protein ASAP1 inhibits cell spreading and migration by influencing Arf1 GTPase cycling. J Biol Chem 280, 8884–8892.

Miller DT, Cagan RL (1998). Local induction of patterning and programmed cell death in the developing *Drosophila* retina. Development 125, 2327–2335.

Morishige M *et al*. (2008). GEP100 links epidermal growth factor receptor signalling to Arf6 activation to induce breast cancer invasion. Nat Cell Biol 10, 85–92.

Nam JM, Onodera Y, Mazaki Y, Miyoshi H, Hashimoto S, Sabe H (2007). CIN85, a Cbl-interacting protein, is a component of AMAP1-mediated breast cancer invasion machinery. EMBO J 26, 647–656.

Onel S, Bolke L, Klambt C (2004). The *Drosophila* ARF6-GEF Schizo controls commissure formation by regulating Slit. Development 131, 2587–2594.

Parker L, Gross S, Alphey L (2001). Vectors for the expression of tagged proteins in Drosophila. Biotechniques 31, 1280–1282, 1284, 1286.

Premont RT, Schmalzigaug R (2009). Metastasis: wherefore arf thou? Curr Biol 19, R1036–R1038.

Randazzo PA, Inoue H, Bharti S (2007). Arf GAPs as regulators of the actin cytoskeleton. Biol Cell 99, 583–600.

Ready DF, Hanson TE, Benzer S (1976). Development of the *Drosophila* retina, a neurocrystalline lattice. Dev Biol 53, 217–240.

Reiter C, Schimansky T, Nie Z, Fischbach KF (1996). Reorganization of membrane contacts prior to apoptosis in the *Drosophila* retina: the role of the IrreC-rst protein. Development 122, 1931–1940.

Rorth P (2009). Collective cell migration. Annu Rev Cell Dev Biol 25, 407–429.

Sabe H (2003). Requirement for Arf6 in cell adhesion, migration, and cancer cell invasion. J Biochem 134, 485–489.

Sabe H, Hashimoto S, Morishige M, Ogawa E, Hashimoto A, Nam JM, Miura K, Yano H, Onodera Y (2009). The EGFR-GEP100-Arf6-AMAP1 signaling pathway specific to breast cancer invasion and metastasis. Traffic 10, 982–993.

Schweitzer JK, D'Souza-Schorey C (2002). Localization and activation of the ARF6 GTPase during cleavage furrow ingression and cytokinesis. J Biol Chem 277, 27210–27216.

Seppa MJ, Johnson RI, Bao S, Cagan RL (2008). Polychaetoid controls patterning by modulating adhesion in the *Drosophila* pupal retina. Dev Biol 318, 1–16.

Tepass U, Harris KP (2007). Adherens junctions in *Drosophila* retinal morphogenesis. Trends Cell Biol 17, 26–35.

Vicente-Manzanares M, Webb DJ, Horwitz AR (2005). Cell migration at a glance. J Cell Sci 118, 4917–4919.

Zeitlinger J, Bohmann D (1999). Thorax closure in *Drosophila*: involvement of Fos and the JNK pathway. Development 126, 3947–3956.